ACS APPLIED MATERIALS & INTERFACES

SPOTLIGHT ON APPLICATIONS

www.acsami.org

Tailoring Mechanical Properties of Aerogels for Aerospace Applications

Jason P. Randall,[†,‡] Mary Ann B. Meador,[*,§] and Sadhan C. Jana[*,†]

[†]Department of Polymer Engineering, University of Akron, Akron, Ohio 44325-0301, United States

[§]NASA Glenn Research Center, Cleveland, Ohio 44135, United States

ABSTRACT: Silica aerogels are highly porous solid materials consisting of three-dimensional networks of silica particles and are typically obtained by removing the liquid in silica gels under supercritical conditions. Several unique attributes such as extremely low thermal conductivity and low density make silica aerogels excellent candidates in the quest for thermal insulation materials used in space missions. However, native silica aerogels are fragile at relatively low stresses. More durable aerogels with higher strength and stiffness are obtained by proper selection of silane precursors and by reinforcement with polymers. This paper first presents a brief review of the literature on methods of silica aerogel reinforcement and then discusses our recent activities in improving not only the strength but also the elastic response of polymer-reinforced silica aerogels. Several alkyl-linked bis-silanes were used in promoting flexibility of the silica networks in conjunction with polymer reinforcement by epoxy.

KEYWORDS: silica aerogel, polymer cross-linking, nanoporous materials, flexible aerogels, sol−gel, conformal coatings, skeletal density

1. INTRODUCTION

Aerogels are highly porous structures formed when the liquid within a gel is replaced by a gas, in such a way that the solid particle networks within the gel do not collapse during the removal of the liquid,[1,2] as shown in Scheme 1. The most common aerogels are silica aerogels, however, aerogels have been made from polymers,[3−6] transition metals,[7−10] and montmorillonite clay/polymer composites.[11,12] Polymeric aerogels have also been pyrolized to form carbon aerogels.[13] Aerogels were first discovered in the early 1930s by Kistler[14,15] while studying gels with a low content of solids. Kistler dispersed colloidal silica particles in water until they became interconnected, and formed a gel network. These gels were observed to support their own weight, but the network collapsed and the gel was destroyed with evaporation of the water under ambient conditions. The surface tension of water pulled on the networks as the liquid meniscus receded during water evaporation and led to destruction of the gel. To resolve this issue, Kistler exchanged the water in the gel with alcohol via a lengthy solvent exchange process and removed the alcohol under supercritical conditions. The resulting materials possessed low density and high porosity, but the process was fairly involved and required high temperature and pressure to remove the alcohol.

Nicolaon and Teichner[16] improved the process of making silica aerogels by employing sol−gel chemistry with tetramethylorthosilicate (TMOS) as the metal alkoxide. The key to the improvement was the use of methanol as the solvent, which was then removed under supercritical conditions. Note that the sol−gel reactions also generated methanol as a byproduct. The direct use of methanol as the solvent avoided the need for the lengthy water to alcohol exchange step as in Kistler's method.[14,15] However, it was still necessary to heat the sample to at least 242 °C for supercritical extraction of the methanol. Hence, another significant advancement in the process of making aerogels was the use of liquid CO_2 in place of methanol as the solvent, which alleviated several concerns associated with supercritical drying of methanol.[17] Super critical conditions with liquid CO_2 can be achieved by heating the system to as low as 32 °C; the required pressure is also slightly lower. The lower temperature in the drying step and nonflammability of CO_2 make the process safer and less expensive.

Regardless of the chemical makeup, aerogels offer many unique properties. Silica aerogels in particular may possess extremely high porosity (>90%), density as low as 2 mg/cm^3,

Scheme 1. Aerogel Fabrication Typically Proceeds through Sol−Gel Process Followed by Supercritical Drying to Avoid Collapsing of the Particle Networks

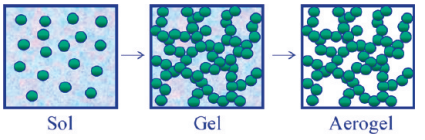

Received: January 3, 2011
Accepted: February 14, 2011
Published: March 01, 2011

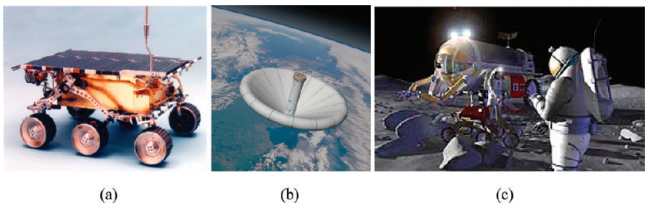

Figure 1. Current and proposed aerospace applications of aerogels, showing (a) Mars rover, (b) an inflatable decelerator concept for EDL applications, and (c) an EVA suit.

and low thermal conductivity (10−30 mW/(m K)) depending on density). However, their load bearing capability is poor and they are easily shattered.[18] A native silica aerogel synthesized from TMOS with an average density of about 120 mg/cm^3 can be completely crushed with the application of stress of about 31 kPa.[19] This fragile nature of silica aerogels became beneficial in several space missions, e.g., in capturing hypervelocity particles of cosmic dust from the tail of a comet.[20,21] The aerogel structure was used to gradually slow particles traveling at high velocity, capturing them intact so that they could be further investigated upon arrival on earth.

Despite their poor mechanical properties, silica aerogels have found use in several applications, including Cherenkov radiators in particle physics experiments[22−24] and thermal insulation for skylights and windows.[25,26] Silica aerogels have also been used for making heat storage devices used in defrosting of windows[27] and as acoustic barrier materials.[28−30] Other aerogels have been demonstrated as battery electrodes,[31,32] catalyst supports,[33,34] and oxygen and humidity sensors,[35,36] taking advantage of their large internal surface areas. However, the fragile nature of native silica aerogels renders them unsuitable for load bearing applications, especially where the external load exceeds the breaking stress. The low values of stress at break in native silica aerogels are often attributed to their unique structure, typically referred to as a pearl necklace or beads-on-a-string organization of spherical secondary silica particles. The secondary particles are connected at neck regions composed of only a few Si−O−Si bonds.

The low values of thermal conductivity and very low density make silica aerogels attractive materials to meet the thermal insulation needs of a number of aerospace applications. Some examples are presented in Figure 1. One example involves insulation around the battery packs in the Mars Sojourner Rover. The aerogel insulation performed admirably, protecting the electronics and the battery for three months—much longer than initially planned.[37] A more robust form of aerogel is desired, however, for more widespread use in aerospace applications. Aerogels are being considered to insulate extra-vehicular activity (EVA) suits for future manned missions to Mars.[38] Aerogel composites are the only materials that come close to meeting the requirements for EVA suit insulation. However, current aerogel composites flake apart under rigorous cyclic loading−unloading tests and lose insulation quality over time.[39,40] Robust aerogel composites are also considered as the baseline insulation materials of inflatable decelerators for entry, descent, and landing (EDL) applications.[41] Inflatable decelerators are proposed to slow spacecraft for planetary EDL.[42] EDL systems used to successfully land six robotic missions on Mars from 1976 to 2008 employed a hard aeroshell heat shield and parachutes of 12−16 m in diameter. Future robotic and manned missions are expected to be much heavier and will require more drag for landing. Hence, new designs with much larger diameters (30−60 m) will be required.[43] The inflatable decelerators need to be stowed in a small space and to deploy into a large area lightweight heat shield to survive reentry.[44] Thus, minimizing the weight and thickness of the system as well as providing suitable insulation capacity are important considerations. Durable, lightweight insulation is also required for applications involving cryogenic storage and transfer systems for vehicle and launch pad operations.[45] Note that aerogels out-perform conventional foam and multilayer insulation systems at ambient pressure and under light vacuum for these applications.

Scheme 2. Typical Approaches to Improving Mechanical Properties of Aerogels; Of These, Only Polymer Reinforcement Builds Conformal Coating on the Particles

The most straightforward way of increasing the strength of aerogels is to increase the density. This is achieved by increasing the total amount of material used in the creation of the gel, thereby increasing the number of connecting points between the secondary particles as shown in Scheme 2. Studies detailing the scaling of mechanical properties with the density of aerogels were put forth by Fricke[46] and Pekala et al.[47] Young's modulus (G) was found to scale with bulk density (ρ_b) in a power law relationship, $G \sim \rho_b^a$, where the exponent, a, is around 3. The value of the exponent was attributed to irregular fractal morphology. Later studies concluded that this scaling relationship was not directly related to fractal morphology, pointing out that a number of aerogels are fractal over less than 1 order of magnitude of length scale. Gross and Fricke illustrated that the scaling range can vary, with a assuming a value between 2 and 4 simply by altering the connectivity of the network.[48] Specifically, the number of dangling ends which do not add to the elasticity of the network impacts the final scaling of modulus with density. Woignier et al.[49] put forth similar arguments, stating that the exponent a does not depend on the fractal nature of the aerogels and that percolation theory is insufficient to describe their results. Instead, gelation, aging, and shrinkage all play roles in defining the final mechanical properties of aerogels. It should be noted that the ambient humidity present during testing can also alter the mechanical properties of silica aerogels, especially for hydrophilic aerogels. Ambient humidity has less of an effect on mechanical properties of hydrophobic aerogels. Miner et al.[50] noted a 60% increase in Young's modulus, from 0.5 to 0.8 MPa, and a 10% increase in mass of hydrophilic silica aerogels due to water vapor uptake.

Another approach to strengthening silica aerogels is to use an aging process. As a silica gel is aged, some monomer leaves the network due to dissolution, and becomes a reactive species again. Silica on the concave curvature (negative radius of curvature) of the neck region between two connected secondary particles is less likely to dissolve than the bulk silica particles.[51] In this manner, the dissolved silica migrates over time to the neck regions within the silane network and precipitates, leading to thickening of the necks. The thickening of the neck regions in turn increases the overall strength of the gel and the final aerogel

product. This phenomenon is known as Ostwald ripening (Scheme 1), and is the basic premise behind any aging phenomena. Note, however, that this route to reinforcement takes a long time under ambient conditions. Ways to expedite the aging process include heat treatment in water,[52] and soaking in alcohol[53,54] with and without additional tetraethyl orthosilicate (TEOS). These processes increased the elastic modulus of the final aerogel products by roughly a factor of 2. More recently, Rolison and co-workers[55] used a combination of aging in methanol and postcuring at 900 °C in air to achieve a 2 orders of magnitude increase in the modulus of aerogels as measured by microindentation. It should be noted that the final aerogel also displayed over a 4-fold increase in density to approximately 0.80 g/cm^3, which is significantly higher than the density of typical aerogels.

Copolymerization or cogellation of silanes with an organic polymer has also been considered as a method of reinforcement. Kramer et al.[56] outlined one of the first successful attempts to reinforce aerogels with polydimethylsiloxane (PDMS). Dubbed aeromosils by these authors, the reinforced aerogels were synthesized from TEOS and varying amounts of PDMS. Some aerogels displayed a 4-fold increase in the compressive strength over neat TEOS-based aerogels and recovered their original shape from a state of 30% compressive strain. Novak et al.[57] mixed preformed poly(2-vinylpyridine) (PVP) with silane precursor prior to gelation and achieved comparable results. Further enhancement of the mechanical properties of the gels was obtained by cross-linking the PVP using Cu(II) salts. Wei et al.[58] used a similar copolymerization approach with poly(vinylpyrrolidone). Martin et al.[59] introduced varying concentrations of polyethylene glycol (PEG) to the sol before gelation and was able to achieve a 50% improvement in modulus with almost no change in the overall density.

Recent studies established that aerogels can be even more effectively strengthened by reacting the hydroxyl groups on the silica gel surface with organic moieties carrying isocyanate groups, followed by supercritical fluid extraction after exchanging solvent with liquid CO_2.[19,60] Unlike the approaches described above, this method leads to a conformal coating of polymer on the silica aerogel backbone as shown in Scheme 2. The resultant aerogels showed large increases in mechanical strength compared to unreinforced silica aerogels when evaluated by three point bending tests. For example, the isocyanate-reinforced aerogels supported stresses up to 800 kPa in a three-point bending test, compared to 20 kPa for a native aerogel of the same density of 280 mg/cm^3. The pore structure, however, did not change much.

More versatile polymer reinforcement can be easily achieved if reactive functional groups are introduced onto the surfaces of the silica gel by coreacting functionalized trialkoxysilanes with conventional silane precursors, such as TMOS or TEOS as shown in Scheme 3.[61] For example, amine functionalities are placed on the surfaces of silica gels by coreacting 3-aminopropyltriethoxysilane (APTES) with TMOS. APTES, due its basic nature, also catalyzes the hydrolysis and condensation of the sol to silica gel as demonstrated by Husing et al.,[62] thus eliminating the need for additional base. These amine-decorated silica gels have been reacted with di-, tri-, and tetra-functional epoxies to obtain a conformal coating of epoxy on the silica network.[63] Similar to the isocyanate-reinforced aerogels[19,64,65] previously discussed, the epoxy-reinforced aerogels showed a 2 orders of magnitude increase in strength over unreinforced silica aerogels.

Scheme 3. Process for Polymer-Reinforcement of Silica Aerogels via Reactive Groups on the Silica Particle Surface; Representative Set of Monomers Used to Obtain Reinforcement Are Presented

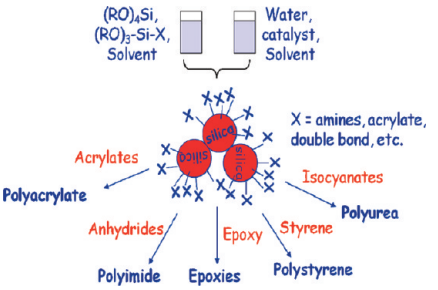

The amine groups on the silica surface also participate in reactions with di-isocyanates, thus producing a reinforcing coating of polyurea. In some cases, this scheme yields more translucent aerogels than can be fabricated by reacting the isocyanates directly with the silanol groups on silica surfaces.[64] The aerogel structures and their properties depend on several factors, such as the concentration of silanes, di-isocyanate cross-linker, initial water concentration, and the number of washes before cross-linking.[65] Statistical methods were used to obtain models relating the physical property data with the above factors. Full quadratic equations were used to fit any nonlinearity in the data. These models can be used as a set of predictors to optimize and refine the morphology of aerogels. A few general trends emerged from the models, in particular, the number of polyurea repeat units between the functional groups increased with the amount of water in the gels. It was found that 18−25 repeat units of polymer produced the largest enhancement in mechanical properties at lower densities than previously reported.[64] The thermal conductivity of optimized aerogels varied from 19 to 36 mW/(m K) as characterized using laser flash method. This showed that the polymer reinforcement does not significantly affect the thermal conductivity of silica aerogels,[66−68] even though surface areas can be reduced by as much as half.

Other variations on reinforcement of silica aerogels with polymer includes styrene-reinforced aerogels,[69−71] and polycyanoacrylate-reinforced aerogels with and without amine surface modification.[72,73] Polyurea-reinforced silica aerogels have also been fabricated with up to 5 w/w % carbon nanofibers as a filler.[74] Polyurea-reinforced aerogel carbon nanofiber composites made using lower total silane concentrations were observed to have higher tensile strength and were easier to handle in the wet gel state before cross-linking and supercritical fluid extraction. In contrast, for aerogel composites produced using the highest silane concentrations, there was little change in the strength because of addition of carbon nanofiber.

A more industrially friendly approach to epoxy reinforcement of aerogels uses ethanol as the solvent in TEOS/APTES aerogels.[75] Previous reinforcement schemes have used less desirable solvents due to limited solubility of the organic cross-linker in common solvents such as ethanol. The process has been further refined into a one-pot reaction scheme, which uses about half the amount of solvent and results in more uniform aerogels in about half the time.[76] Notably, these epoxy-reinforced aerogels have comparable compressive modulus at the same density to previously optimized polyurea-reinforced aerogels. However, the surface areas obtained from Brunauer-Emmet-Teller (BET)

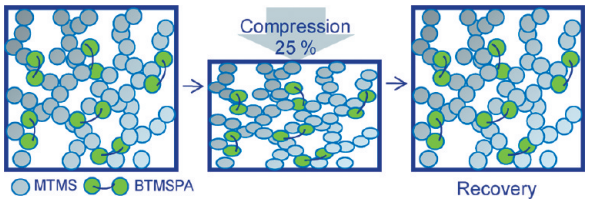

Figure 2. Schematic of MTMS and BTMSPA-derived polyurea-reinforced aerogels showing recovery after compression.

analysis for these aerogels are more than double compared to polyurea-reinforced aerogels (300−350 vs 150 m^2/g). Note that higher BET surface areas are typically a good predictor for lower thermal conductivity in aerogels.

Although polymer-reinforced silica aerogels provide good compressive strength, it is apparent that the manufactured articles must be cast in their final forms as the aerogels cannot be reshaped due to brittleness under large deformation. Though the polymer-reinforced aerogels at densities below 0.06 g/cm^3 can be deformed to a bend of about 50° without breakage,[77] it has been shown that the flexibility/elasticity of silica networks can be more greatly enhanced by altering the SiO_2 backbone in some significant way. The aeromosils reported by Kramer et al.[56] with PDMS links within the SiO_2 backbone showed some degree of recovery after compression. PDMS linked silica aerogels have also been produced in thin film form and reinforced with electrospun nanofibers of flexible polyurethane.[78] These aerogels were extremely bendable and flexible, with the electrospun fibers bridging any small cracks that formed. Rao and co-workers[79] used methyltrimethoxysilane (MTMS) in preparation of aerogels by a two-step process. The first step involved hydrolysis under acidic conditions and the second step involved condensation with a base catalyst. The authors observed that the aerogel could be bent almost back upon itself, i.e., to approximately a 180° bend. In addition, the aerogel recovered its original length from a state of almost 60% compression, although not much force was required to compress the sample. This was attributed to decreased bonding in the silica network, since MTMS can undergo condensation at only three points instead of four as in the cases of TMOS or TEOS. Similar results were reported by Kanamori et al.[80] and Bhagat et al.,[81] who showed that this spring-back behavior could be used to dry the gels under ambient conditions and to yield xerogels with nearly the same pore structure as the corresponding supercritically dried aerogels. Notably, the MTMS aerogels produced by Kanamori et al. using supercritical fluid extraction were exceptionally clear, having light transmission in excess of 90%.

Simultaneous alteration of the silica backbone and reinforcement of the gel structure using a conformal coating of polymer as shown in Figure 2 resulted in spring-back behavior as well as stronger aerogels. For example, aerogels obtained by coreacting MTMS with bis(trimethoxysilylpropyl)amine (BTMSPA) and reinforcing with polyurea have been recently reported.[82] Both MTMS and BTMSPA contribute to the reduction of stiffness of the silica backbone through reduced Si−O−Si bonding per molecule and due to inclusion of a flexible alkyl linking group. On the other hand, BTMSPA provides a secondary amine for reaction with an isocyanate (Desmodur N3300, Bayer), thus anchoring a polyurea conformal coating on the silica networks. The resulting polyurea-reinforced aerogels showed good recovery, e.g., to less than 1% unrecovered strain from a state of 25% compression over a wide range of compressive modulus (up to 150 MPa). In addition, the polyurea-reinforced aerogels exhibit an order of magnitude improvement in stress at break and toughness over the unreinforced aerogels, and BET surface area greater than 200 m^2/g.

Similar but less dramatic results have been reported for epoxy-reinforced aerogels synthesized by replacing up to 40% of the TEOS or TMOS in the silica backbone with alkyl linked bis(trimethoxysilyl)hexane (BTMSH). The BTMSH reduces stiffness in the silica backbone by replacing some of the more rigid Si−O−Si bonds with flexible hexyl links. The resultant epoxy-reinforced aerogels provided modulus up to 23 MPa[75,76] and almost complete recovery from a state of 25% compressive strain.

Styrene-reinforced aerogels containing BTMSH also showed good recovery from compression, but the modulus of these aerogels were lower, only up to 3 MPa. An increase in BTMSH concentration in the formulations also led to inhibition of cross-linking through vinyl groups on the silica surface.[71] Non-cross-linked aerogels[83] made from a combination of TMOS and bis[3-(triethoxysilyl)propyl]disulfide, the latter a source of flexible silane linking group, also showed almost complete recovery from 25% compression with a similar modulus (4 MPa) and density (0.2 g/cm^3). A high proportion of the disulfide in the formulation yielded lower density monoliths, which recovered completely from as much as 75% compression, although the modulus was quite low and the surface area was greatly reduced. Nonpolymer-reinforced aerogels made from the alkyl-linked silsesquioxanes, including ethyl-linked bis(triethoxysilyl)-ethane (BTESE), hexyl-linked bis(trimethoxysilyl)-hexane (BTMSH), and octyl-linked bis(triethoxysilyl)octane (BTESO) have been examined previously by Loy, Shea, and co-workers.[84−88] These studies focused on porosity and relative surface areas of the resulting silsesquioxane aerogels as well as reactivity of the precursors. However, little data has been published on the mechanical properties of these aerogels.

2. CURRENT RESEARCH

Above, we examined several cross-linking schemes and different methods of introducing flexibility to the silica backbone and eliciting elastic response from the aerogel monoliths. However, no systematic study exists in literature that examines the relative merits of different silica backbones using a single type of polymer reinforcement. Thus, fundamental questions remain concerning the relative contributions of silica backbones to the properties of aerogels, independent of the type of polymer reinforcement and the nature of reactive functional groups used. In this light, our current work, as shown in Scheme 4, uses only one epoxy (bisphenol A proposylate diglycidyl ether) as the reinforcement and examines the effects of different alkyl-linked bis-silanes, as well as the use of dimethyldiethoxysilane (DMDES) as ways of altering the silica backbones. In addition, the study considers a direct comparison of the performance of amine reactive sites derived from APTES and BTMSPA. We present preliminary results on the effect of the variables mentioned above on density, pore structure, modulus, and elastic recovery of epoxy-reinforced aerogels.

In the first part of the discussion, we focus on three different silane precursors all containing organic linking groups, such as ethyl-linked BTESE, hexyl-linked BTMSH, and octyl-linked BTESO. This elucidates if there is an optimal length of an

Scheme 4. Reaction Scheme for Epoxy-Reinforced Aerogels Incorporating Two Different Amines and Four Types of Flexible Linking Groups in the Silica Backbone

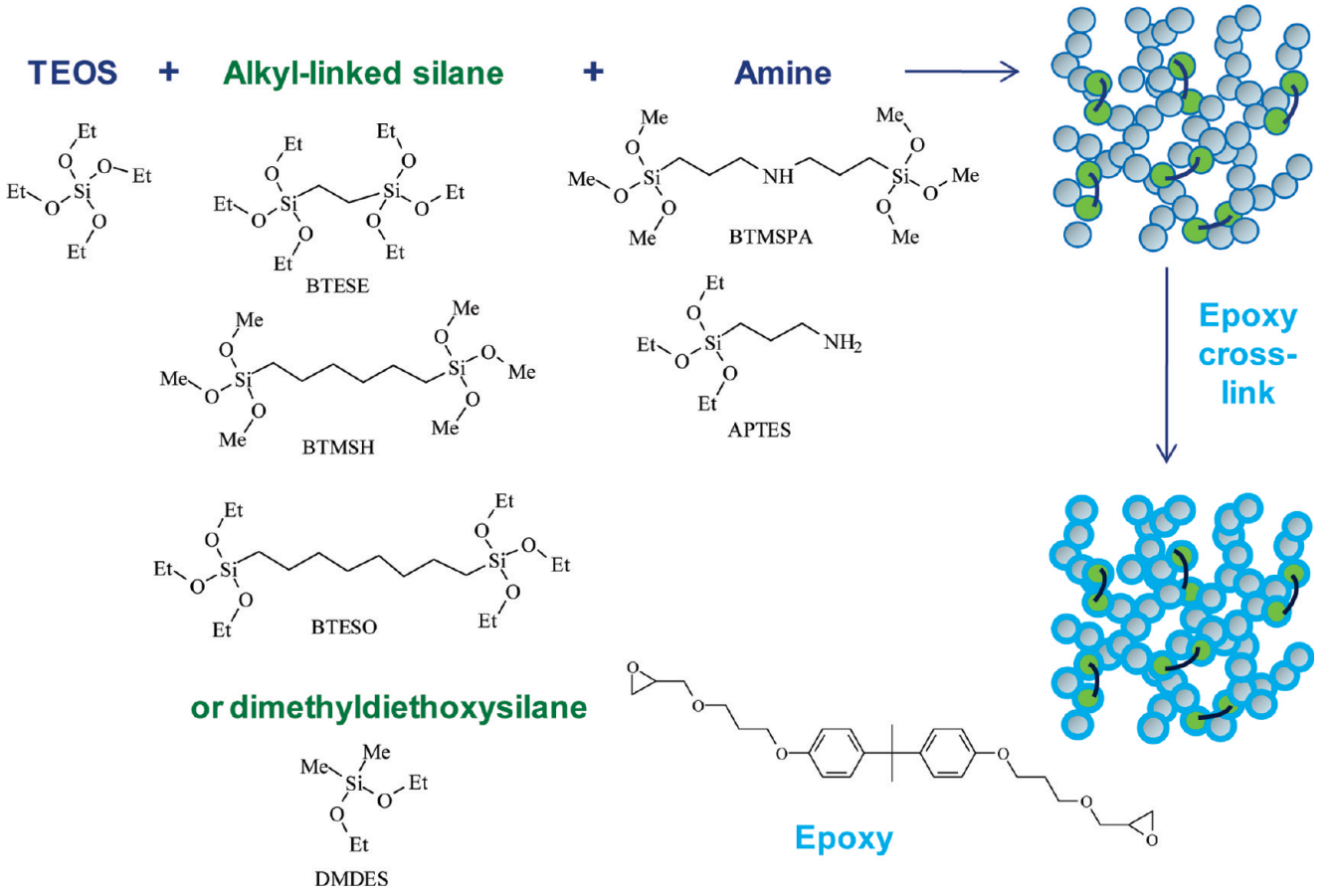

organic linking group in the silica backbone, which would give rise to the highest modulus and optimum elasticity. In the second part, we explore reducing the number of Si−O−Si bonds by using a difunctional silane, DMDES, in order to improve the elastic response. The impact of alternative amines for silica surface modification and reaction with epoxy is also examined.

2.1. Alkyl-Bridged Silanes. Three organic linking groups were examined, BTESE, BTMSH, and BTESO, respectively with two, six, and eight carbon atoms in the alkyl chains. Two amine containing silanes, APTES and BTMSPA were also selected for comparison. All silanes were purchased from Gelest, Inc. (Morrisville, PA). Bisphenol A propoxylate diglycidyl ether (epoxy) and 200-proof ethanol were acquired from Sigma-Aldrich. All components were used as received without further purification.

The method of synthesis for the epoxy-reinforced aerogel monoliths is similar to the process described by Meador et al.[75] and is outlined in Scheme 4. Mole fractions of the ingredients were calculated based on the total moles of Si atoms in the gel network. The total moles of silicon were used instead of total moles of silane as each mole of BTMSPA, BTESE, BTMSH, and BTESO contribute two moles of silicon to the final network, whereas TEOS and APTES contribute only one. Previous research indicates that silicon concentration has a strong impact on all properties of the aerogels.[19,63,64,74,75] Hence the silicon concentration was kept constant in all silane formulations. However, this means APTES containing aerogels had twice as many amines compared to aerogels from BTMSPA for a given mole fraction of total silicon. TEOS content was adjusted to achieve a total Si concentration of 1.6 mol/L after adding together the amounts of amine containing silane (APTES or BTMSPA), and alkyl linked silane (BTESE, BTMSH, or BTESO). In addition, a water-to-Si mole ratio of 3:1 (4.8 mol/L of water) was used in all formulations.

A sample procedure for epoxy-reinforced aerogel synthesis is given below.[89] A solution consisting of TEOS, water, nitric acid, and ethanol was stirred for 1 h and chilled in a dry ice/acetone bath. The chilled solution was combined with another chilled solution of APTES and BTESE in ethanol, and stirred vigorously. The resulting sol was then poured into cylindrical molds and allowed to gel and age at room temperature over a period of 24 h. The gels were removed from the mold and dipped in fresh ethanol at room temperature, left for 24 h, and then washed again with fresh ethanol to remove water or methanol byproduct. After soaking for an additional 24 h, the gels were dipped in a solution of 20% (w/w) bisphenol A propoxylate diglycidyl ether in ethanol and allowed to soak for 24 h. This allowed time for diffusion of epoxy molecules into the gel network and to participate in epoxy-amine reactions. The excess monomer in solution was subsequently exchanged for fresh ethanol and the gels in ethanol were heated at 70 °C for 3 days. Afterward, the gel was rinsed four times in ethanol to remove any unreacted epoxy

and dried in a supercritical CO_2 chamber. In the supercritical drying process, the sample specimens were rinsed five times in liquid CO_2, each rinse taking 1.5 h at a gas flow rate of 4.0 L/min, with a half-hour soak time in between the rinses. The temperature of the vessel was then raised from ambient to 65 °C over the course of about 45 min and the supercritical CO_2 was vented out. After supercritical drying, the samples were outgassed under a vacuum at 60 °C for 24 h to remove any residual solvent. Unreinforced aerogel specimens were made using the method described above with the following exception—the gels were rinsed four times in ethanol prior to supercritical drying.

First, to gain insight into the effect of the different silanes on the silica backbone, we examined unreinforced aerogels. The observed mass of silica and organics in the aerogels is an indicator of the reactivity of the silane precursors (hydrolysis and condensation) and how well they are incorporated into the backbone. In view of this, the yield for unreinforced silica aerogels was determined by dividing the observed mass by the theoretical mass. The theoretical mass refers to the mass of completely hydrolyzed and condensed silica aerogels. Note that yields in excess of 100% reflect incomplete hydrolysis and/or condensation of silanes incorporated in the silica backbone. On the other hand, yields of less than 100% indicate loss of silanes. This can occur if oligomers or cyclic products of the silanes not covalently bonded to the gel are removed during washing steps or supercritical drying. The yields of aerogels derived from the two amines—APTES and BTMSPA—are compared in Figure 3. Empirical models derived from a larger data set including other formulations with additional amine concentrations (not discussed here) are plotted as lines on the graphs. Figure 3a compares the yields obtained for unreinforced aerogels comprised of 35 mol % APTES for 0—45 mol % of each of the bis-silanes. It is observed in Figure 3a that when BTMSH is used, the yield is a little above 100% and independent of BTMSH concentration in the aerogel formulations. This indicates that for BTMSH, the yield is very close to theoretical for all formulations, meaning that no appreciable silane is lost during formation of the organic-silica backbone. In contrast, for unreinforced aerogels made using BTESE, the yield decreased dramatically to about 80% of the theoretical yield for the highest mole fraction of bis-silane studied. This mass loss is consistent with observations by Loy and co-workers[85] that cyclic dimers and trimers readily form with ethyl linked bis-silane. For aerogels made using BTESO the mass loss was even more severe (~40% yield at 45 mol % BTESO). This may be due to lower reactivity of the octyl linked silane to base catalyzed condensation as observed previously by silicon NMR[90] and subsequent loss of oligomers during processing.

The same comparison of yields obtained for unreinforced aerogels containing 50 mol % BTMSPA is shown in Figure 3b. This graph follows the same overall trends observed in Figure 3a, although the loss of silane in aerogel formulations containing up to 45 mol % silicon from BTESO is much less than those based on APTES (55% yield). This difference could be due to the lower basicity of the sols because BTMSPA contains a secondary amine and there is a little less amine in the formulation.

Scanning electron micrographs (SEMs) of aerogels from this study are shown in Figure 4. Unreinforced aerogels made from 50 mol % BTMSPA (4a) and no alkyl linking groups have a finer pore structure than the corresponding epoxy-reinforced aerogels with the same silica backbone (4c). The corresponding pair made with 35 mol % APTES (4b unreinforced, and 4d epoxy-reinforced) appear almost identical in morphology. Note also the density of the epoxy-reinforced aerogels increased only 40—50% over the unreinforced aerogels, whereas surface area decreased by about half.

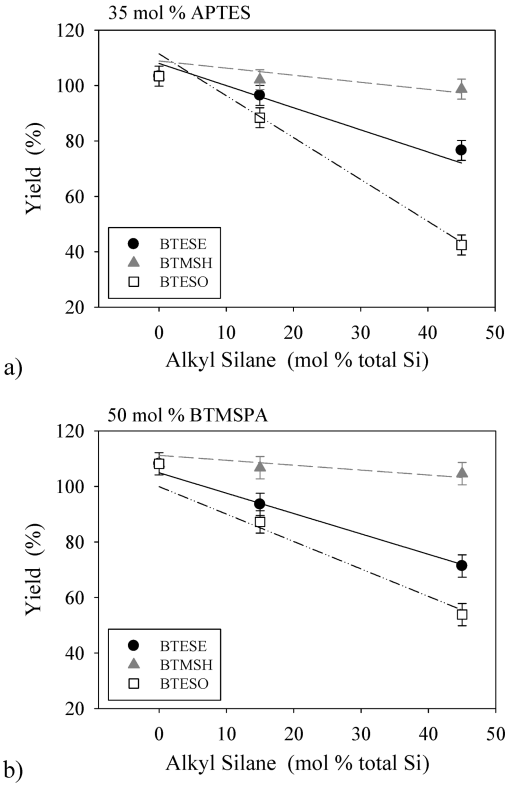

Figure 3. Yield of unreinforced silica aerogels made using (a) 35 mol % APTES and (b) 50 mol % BTMSPA, graphed as a function of increasing alkyl bis-silane concentration. The lines represent empirical models based on a larger data set. Error bars represent one standard deviation derived from the models.

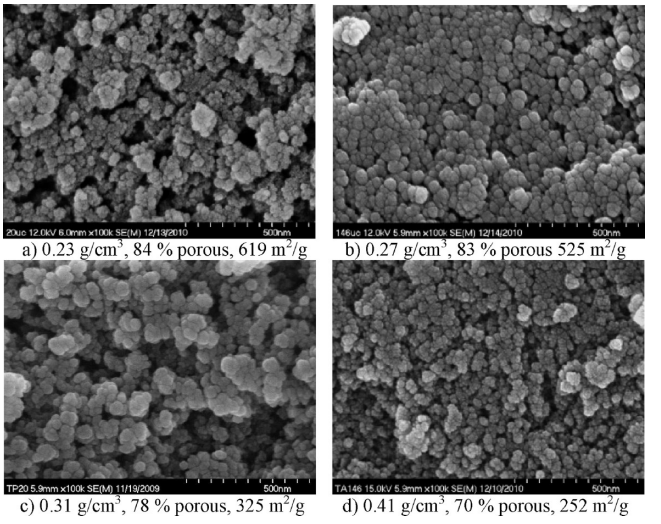

Figure 4. Scanning electron micrographs of unreinforced aerogels from (a) 50 mol % BTMSPA and (b) 35 mol % APTES, and epoxy-reinforced aerogels from (c) 50 mol % BTMSPA, and (d) 35 mol % APTES (no alkyl-linked bis-silanes).

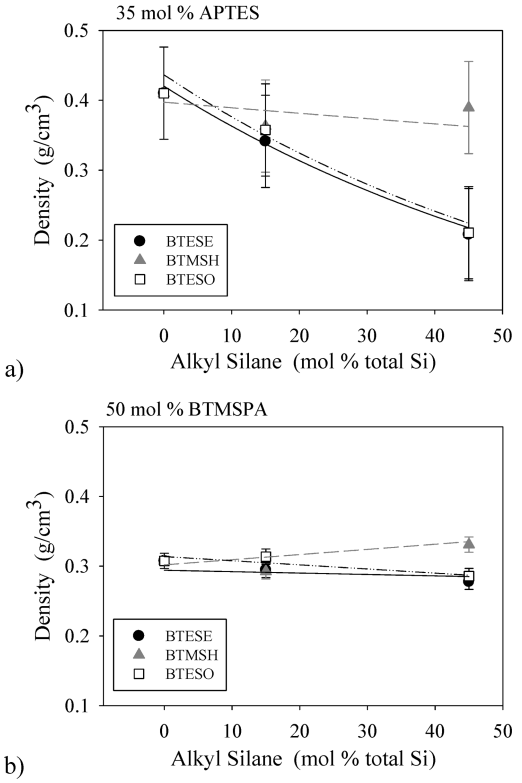

Figure 5. Bulk density of epoxy-reinforced aerogels as a function of alkyl silane concentration for (a) 35 mol % APTES and (b) 50 mol % BTMSPA. The lines are empirical models based on a larger data set with error bars reflecting one standard deviation from the models.

Loss of silane precursors during the fabrication influences the densities of the epoxy-reinforced aerogels, along with other factors. The variation in bulk density of aerogel specimens as a function of bis-silane fraction is presented in Figure 5. For aerogels derived from APTES and ethyl-linked (BTESE) or octyl-linked (BTESO) silanes, density decreases with increasing bis-silane concentration as seen in Figure 5a, but remains nearly constant for hexyl-linked (BTMSH) silanes. This is generally consistent with the loss of silane derived from the yields of the same formulations of unreinforced aerogels. However, recall from Figure 3a that yields for BTESE and BTESO derived aerogels differed significantly, while densities for these aerogels in Figure 5a is nearly the same. This is primarily due to differences in shrinkage between BTESE and BTESO derived aerogels—BTESO aerogels shrink more during the process, increasing the density beyond what is expected when considering yield.

It is surprising that the density of the hexyl-linked (BTMSH) aerogels decreased slightly with increasing mole percentage of silicon from the bis-silane. Since yields from Figure 3a did not change much, it would be expected that density would increase with increasing BTMSH fraction, due to the additional mass of the hexyl-linkages. The observed decrease in density is a result of less shrinkage with increasing BTMSH fraction. Epoxy-reinforced aerogels made using BTMSPA as amine do not shrink as much as APTES aerogels in response to increasing the bis-silane fraction. Hence, the plot in Figure 5b does show an increase in density with increasing BTMSH. Differences in shrinkage also account for the near constant density shown in

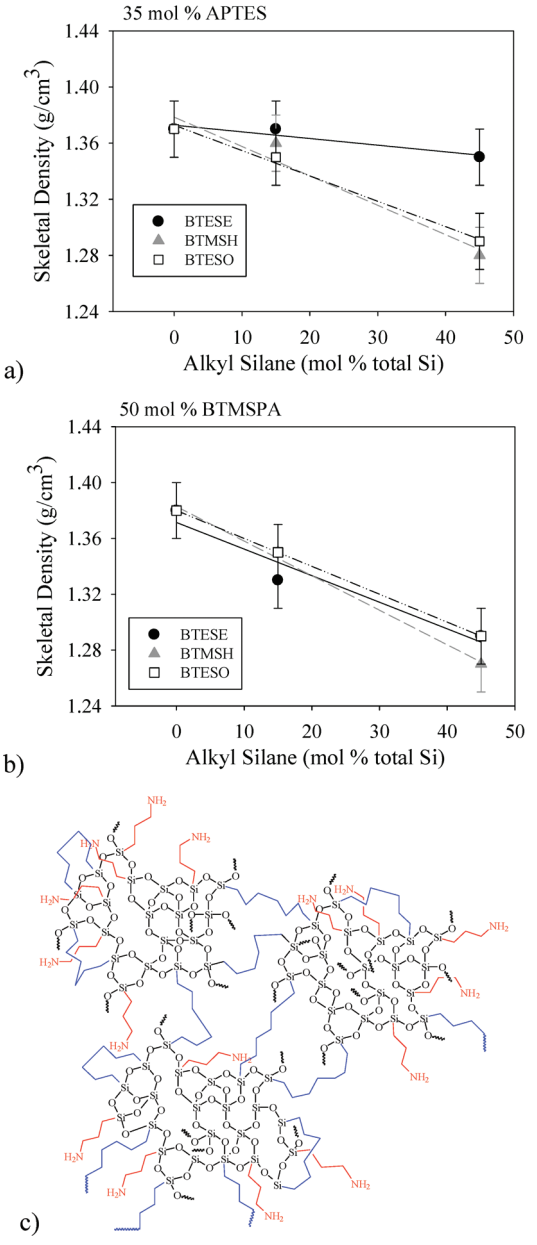

Figure 6. Skeletal density of epoxy-reinforced aerogels as a function of alkyl silane concentration for (a) 35 mol % APTES, (b) 50 mol % BTMSPA, and (c) proposed molecular structure of a silica backbone made from TEOS, APTES, and BTMSH.

the plot in Figure 5b obtained for epoxy-reinforced aerogels made from a combination of BTMSPA with BTESE or BTESO.

The skeletal density of epoxy-reinforced aerogels derived from the three bis-silanes and measured by helium pycnometry is presented in Figure 6. The skeletal density is dependent on the packing of the various bis-silanes in the primary and secondary particles. It is seen that the skeletal density decreased slightly with increasing concentration of BTESE for aerogels derived from APTES (Figure 6a), whereas a more pronounced decrease with BTMSH and BTESO concentration was observed. In aerogels derived from BTMSPA (Figure 6c), increasing concentration of all three alkyl-linked bis-silane fraction decreased the skeletal density. These results indicate that the primary and secondary particles in aerogels with higher bis-silane concentration are

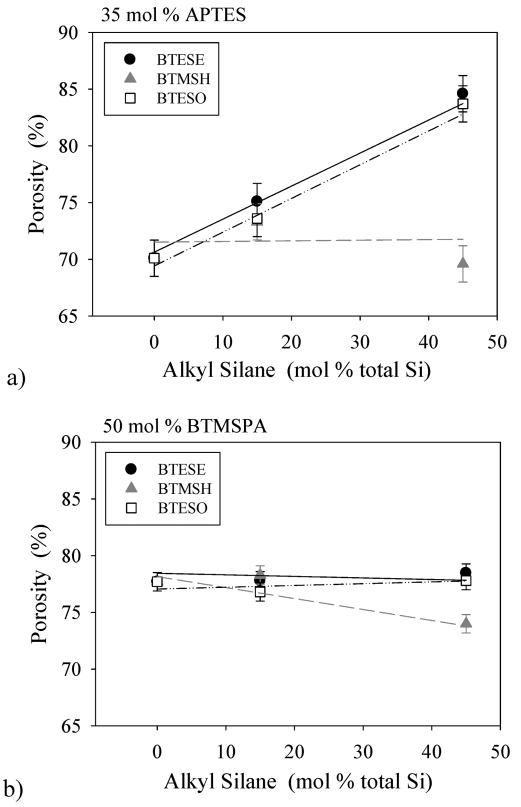

Figure 7. Porosity of epoxy-reinforced aerogels as a function of alkyl silane concentration for (a) 35 mol % APTES and (b) 50 mol % BTMSPA. The lines are empirical models based on a larger data set with error bars reflecting one standard deviation from the models.

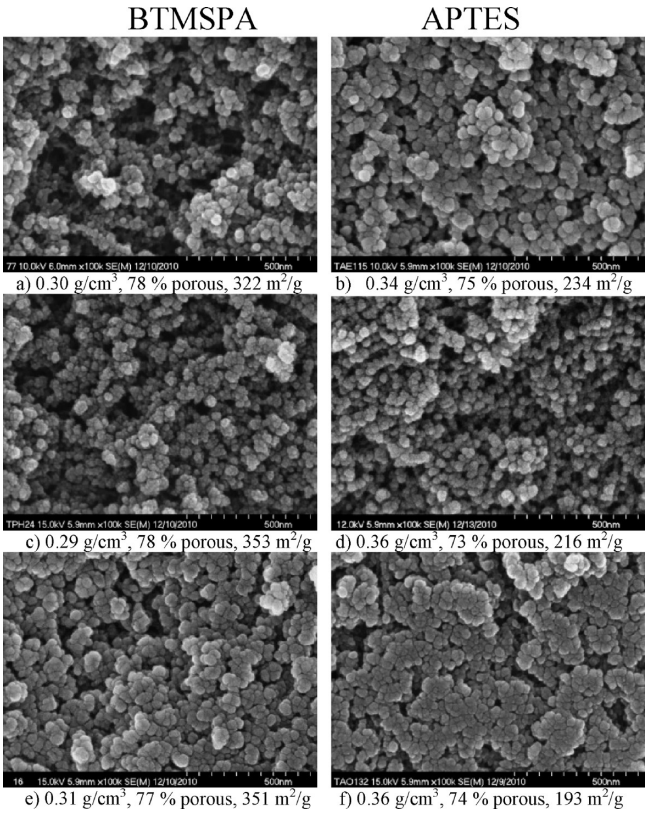

Figure 8. Scanning electron micrographs of epoxy-reinforced aerogels from 15 mol % BTESE with (a) 50 mol % BTMSPA and (b) 35 mol % APTES; from 15 mol % BTMSH with (c) 50 mol % BTMSPA and (d) 35 mol % APTES; and from 15 mol % BTESO with (e) 50 mol % BTMSPA and(f) 35 mol % APTES.

more loosely packed as shown for example in Figure 6c for a silica backbone made using BTMSH, APTES, and TEOS.

The porosity of the epoxy-reinforced aerogels was calculated using eq 1, where ρ_s is the skeletal density determined from helium pycnometry and ρ_b is the bulk density. Porosity ranged from 70 to 85% for all epoxy-reinforced aerogels studied. The porosity of aerogels synthesized from alkyl-linked silanes and from APTES and BTMSPA is shown in panels a and b in Figure 7, respectively.

$$\text{porosity} = 1 - \frac{\rho_b}{\rho_s} \quad (1)$$

Because the skeletal density varies only about 9−10% over the whole range studied, whereas bulk density doubles over the same range, the trends for porosity are nearly the mirror image to those for bulk density. Hence, as shown in Figure 7a, an increase in BTESE or BTESO fraction in APTES aerogels increased the porosity. Also, increasing the hexyl-linked BTMSH concentration had little effect on the porosity of APTES aerogels. These aerogels exhibited an overall lower porosity than aerogels with ethyl- or octyl-linkages. For aerogels made using BTMSPA, porosity remained relatively constant with increasing alkyl-linked silane concentration for both BTESE and BTESO formulations (Figure 7b). Increasing concentration of BTMSH in BTMSPA aerogels slightly reduced the porosity.

A comparison of scanning electron micrographs of epoxy-reinforced aerogels made using 15 mol % of the alkyl linked silanes is shown in Figure 8. The BTMSPA-derived samples (Figure 8, left) are slightly less dense and more porous than the corresponding APTES samples (Figure 8, right) because of the lower amine content in the BTMSPA aerogels, leading to less epoxy cross-linking as previously discussed. Other than this slight difference in porosity, the aerogels made from ethyl-linked silanes (Figure 8a,b) are very similar in particle size and arrangement of the pores. Aerogels made with hexyl-linked silanes (Figure 8c,d) appear to have the finest arrangement of particles, whereas the aerogels derived from octyl-linked silanes have the coarsest particle structure.

Epoxy-reinforced aerogels made using BTMSPA also exhibited higher surface areas as measured by nitrogen sorption data analyzed using the Brunauer−Emmett−Teller (BET) method. Graphs of surface area vs alkyl silane concentration are shown in Figure 9. In general, as seen in Figure 9a, all APTES derived aerogels showed a decrease in surface area with increasing alkyl-linked silane. For BTMSPA derived aerogels (Figure 9b), ethyl- and octyl-linked silanes had no effect on the surface area, whereas increasing the concentration of hexyl-linked silanes slightly increased the surface area.

Compressive modulus is directly impacted by bulk density in aerogels as previously discussed. The values of compressive modulus for various alkyl-linked bis-silanes are plotted in Figure 10. In Figure 10a, it is observed that for epoxy-reinforced aerogels containing APTES, the compressive modulus decreased from 100 MPa to about 10 MPa with the increase of bis-silane concentration for both BTESE and BTESO derived aerogels.

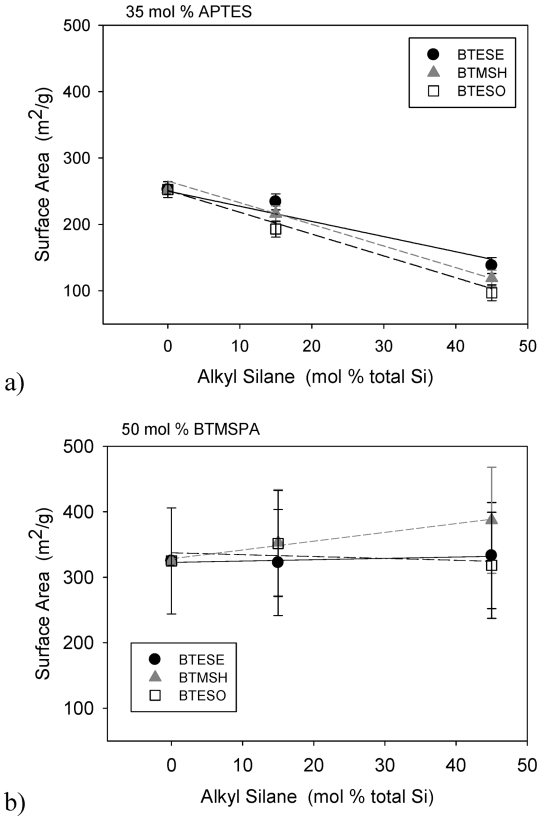

Figure 9. Surface areas of epoxy-reinforced aerogels from BET analysis as a function of alkyl silane concentration for (a) 35 mol % APTES and (b) 50 mol % BTMSPA. The lines are empirical models based on a larger data set with error bars representing one standard deviation derived from the models.

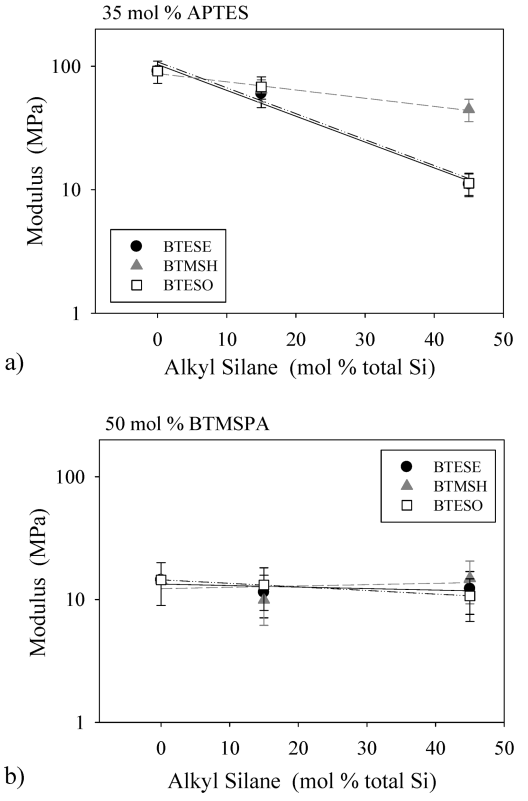

Figure 10. Compressive modulus of epoxy-reinforced aerogels for (a) 35 mol % APTES and (b) 50 mol % BTMSPA, as a function of increasing alkyl silane concentration. Error bars represent one standard deviation from the models.

This reduction in modulus can be attributed to lower density observed with increasing alkyl-linked silane content. The modulus of BTMSH-based aerogels decreased only slightly (Figure 10a), reflecting the near constant density over the same range. On the other hand, for BTMSPA derived aerogels, the compressive modulus was low (~10−20 MPa), and did not change with bis-silane concentration (Figure 10b) for any of the formulations, also in line with the trend observed for bulk density.

The recovery from compressive strain was studied as a means of assessing the flexibility of the aerogel specimens. The load on each epoxy-reinforced aerogel sample was released immediately after compression to 25% strain and allowed to undergo strain recovery for a period of 30 min. The 25% compressive strain was applied at a rate of 1.27 mm/min. The unrecovered strain was obtained by dividing the difference between the initial length and the final length of the specimen by the initial length. A lower value of unrecovered strain indicates better recovery and more elastic response from the aerogel. An unrecovered strain of 0% indicates perfectly elastic response. If a specimen broke during compression, it was assigned an unrecovered strain of 25%, the maximum compressive strain.

The data in Figure 11a indicate that the epoxy-reinforced aerogels containing APTES became more elastic with increasing addition of any bis-silane. The aerogel without any alkyl-linked silanes suffered brittle failure prior to reaching a 25% strain.[91] The use of as little as 15 mol % alkyl-linked bis-silanes with APTES allowed the specimens to undergo 25% compressive deformation without failure and to obtain unrecovered strains of 1 to 2%. Interestingly, all aerogel specimens containing BTMSPA underwent 25% deformation without breakage. The specimens without bis-silanes showed near perfect recovery, while the addition of alkyl bridged silanes slightly hindered the recovery process, and unrecovered strain increased with bis-silane concentration to 4−10% (Figure 11b). Hence, elastic recovery is enhanced more by simply replacing APTES with BTMSPA than by additional use of other alkyl linked silanes.[91] On the other hand, as previously noted, modulus is reduced more in epoxy-reinforced aerogels using BTMSPA. Thus, a combination of higher modulus and a high degree of elastic recovery is obtained with epoxy-reinforced aerogels using APTES and 15 mol % BTMSH. However, it should be noted that the surface area is lower, perhaps leading to higher thermal conductivity for the same density aerogel. Hence, the properties required for a given application need to be considered carefully when choosing the aerogel backbone.

2.2. DMDES Aerogels. We turn now to the impact of adding a difunctional silane, such as DMDES, instead of the alkyl-linked silanes discussed above. Difunctional silanes can produce only two Si−O−Si linkages per molecule compared to four and six Si−O−Si linkages with TEOS and the bis-silanes, respectively. This was anticipated to reduce the stiffness of silica networks, in much the same way that MTMS, with three Si−O−Si linkages is observed to do in unreinforced aerogels[79−81] and polyurea-reinforced aerogels.[82] Sample specimens were made by substituting up to 45 mol % TEOS with DMDES.

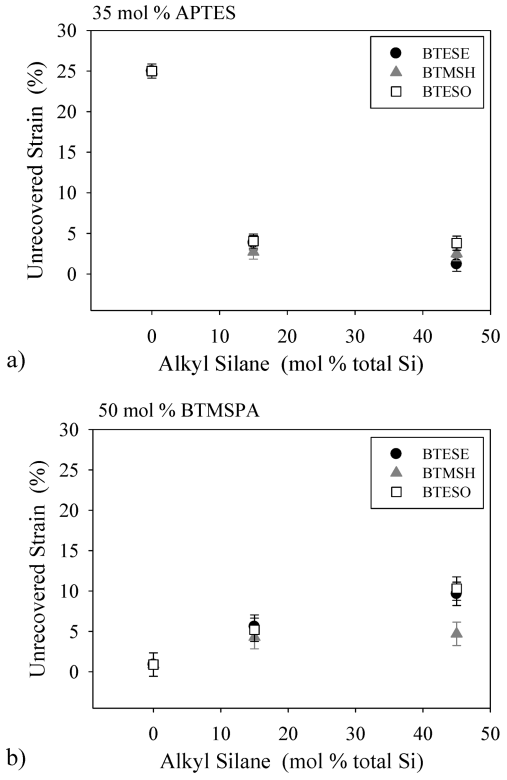

Figure 11. Unrecovered strain of epoxy-reinforced aerogels for (a) 35 mol % APTES and (b) 50 mol % BTMSPA, as a function of increasing alkyl silane concentration. Error bars represent one standard deviation from the models.

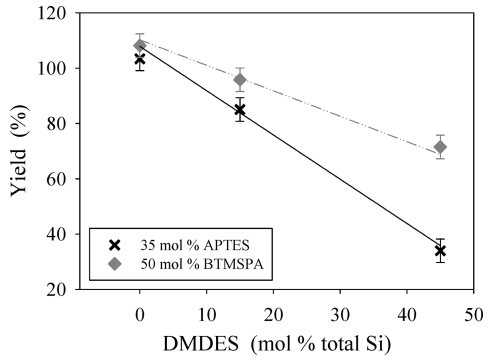

Figure 12. Yield of native silica aerogels as function of DMDES concentration. The lines are empirical models based on a larger data set with error bars reflecting one standard deviation from the models.

It is seen in Figure 12 that mass yield was reduced significantly with increasing the amount of DMDES in the unreinforced aerogels. Such a decrease was greater in aerogels containing APTES than in less basic BTMSPA derived aerogels. This is again attributed to loss of oligomers and cyclic products not covalently bonded to the gel structure, during washing and supercritical fluid extraction steps. The difunctional DMDES contributes toward linear chain growth and not to the network structure. In this way, it is possible that the silica particles become effectively capped with dimethylsiloxy and amine groups before all silane precursors have reacted.

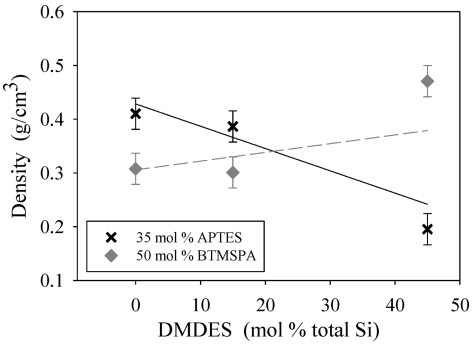

Figure 13. Bulk density of epoxy-reinforced aerogels as function of DMDES concentration. The lines are empirical models based on a larger data set with error bars reflecting one standard deviation from the models.

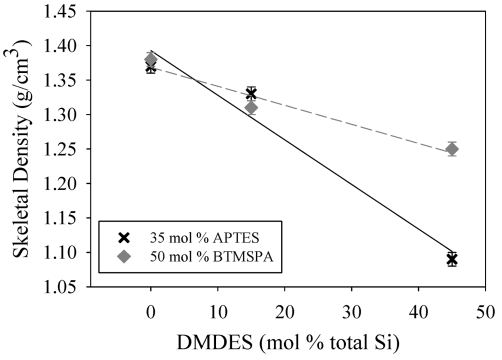

Figure 14. Skeletal density of epoxy-reinforced aerogels as function of DMDES concentration. Error bars represent one standard deviation derived from the models.

Graphs of bulk density of epoxy-reinforced aerogels with DMDES are shown in Figure 13. The density of aerogels containing APTES decreased with increasing DMDES fraction which is attributed to mass loss observed with increasing DMDES fraction as already discussed in Figure 12. In contrast, the density of aerogels containing BTMSPA increased with an increase in DMDES fraction. Again, this can be attributed to less shrinkage and higher mass yields in the BTMSPA aerogels and the fact that additional methyl groups from DMDES should contribute to higher density.

Graphs of skeletal densities of epoxy-reinforced aerogels plotted vs DMDES mole fraction are presented in Figure 14. BTMSPA-derived aerogels show decrease in skeletal density with increasing DMDES fraction, but the decrease is even more pronounced with APTES aerogels. The graphs of porosity of the epoxy-reinforced aerogels shown in Figure 15 again are the mirror images of the bulk density plots. In BTMSPA-derived epoxy-reinforced aerogels, porosity increases and bulk density decreases with increasing DMDES fraction (Figure 13). In contrast, epoxy-reinforced aerogels containing APTES are only slightly lower in porosity with increasing the amounts of DMDES.

Scanning electron micrographs of epoxy-reinforced aerogels made using 15 mol % DMDES are shown in Figure 16. The two micrographs are very similar with slightly larger particle sizes and larger pores in the BTMSPA derived aerogel sample (Figure 16a) compared to that of the APTES sample (Figure 16b). As

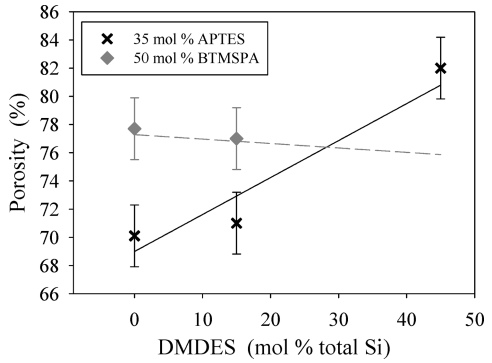

Figure 15. Porosity of epoxy-reinforced aerogels as function of DMDES concentration. The lines are empirical models based on a larger data set with error bars reflecting one standard deviation derived from the models.

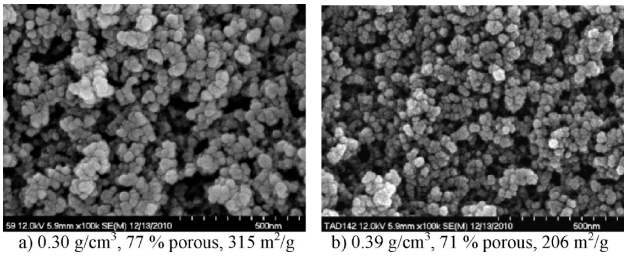

Figure 16. Scanning electron micrographs of epoxy-reinforced aerogels made using 15% DMDES with (a) 50 mol % BTMSPA, and (b) 35 mol % APTES.

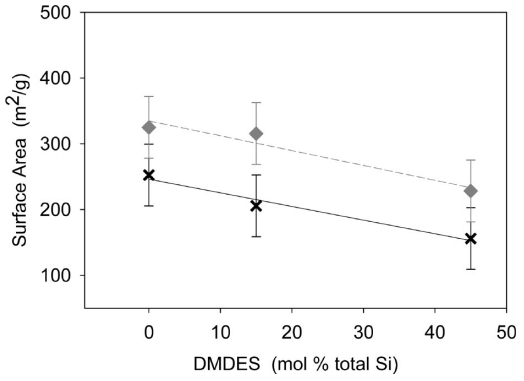

Figure 17. Surface area of epoxy-reinforced aerogels graphed as a function of DMDES concentration. The lines are empirical models based on a larger data set with error bars reflecting one standard deviation derived from the models.

observed with the alkyl-linked silanes, BET surface areas are 100 m^2/g higher for epoxy-reinforced aerogels made from BTMSPA compared to APTES. Also as seen in the plot of surface area vs DMDES mol fraction in Figure 17, increasing DMDES fraction leads to lower surface area for both APTES and BTMSPA derived aerogels.

Figure 18 shows graphs of compressive modulus of the epoxy-reinforced aerogels plotted with DMDES fraction. Once again the aerogels containing APTES displayed higher modulus than those derived from BTMSPA at lower DMDES concentrations. The modulus decreased substantially from close to 100 MPa in

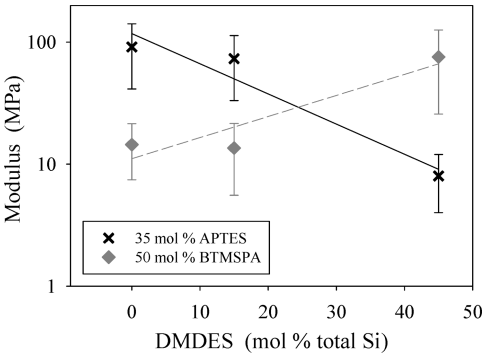

Figure 18. Compressive modulus of epoxy-reinforced aerogels graphed as a function of DMDES concentration. The error bars represent one standard deviation from the models.

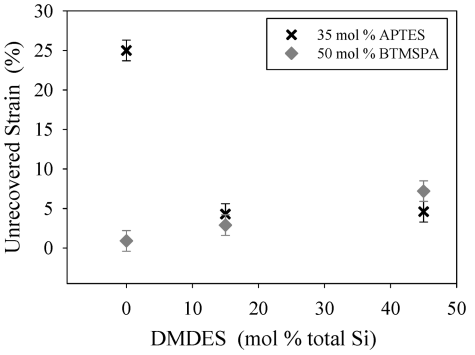

Figure 19. Unrecovered strain of epoxy-reinforced aerogels graphed as a function of DMDES concentration. The error bars represent one standard deviation from the models.

the absence of DMDES to approximately 10 MPa with incorporation of 45 mol % of DMDES. Some reduction in modulus is expected due to fewer Si−O−Si bonds produced from DMDES, which reduces the interconnectivity of the silane network and is also reflected by the 30% reduction in skeletal density for APTES derived aerogels. The loss of silane with increasing DMDES concentration also contributed to the lower modulus. On the other hand, increasing DMDES concentration in epoxy-reinforced aerogels derived from BTMSPA led to an increased modulus, most likely due to higher density observed in this formulation (Figure 13).

Figure 19 shows how the unrecovered strain changed as a function of DMDES concentration. Recall that epoxy-reinforced aerogels derived from APTES without DMDES exhibited brittle facture before reaching 25% compressive strain. Interestingly, the presence of 15 mol % or higher DMDES in APTES-derived aerogels was enough to prevent brittle failure up to 25% compressive strains and to improve elastic recovery. It is inferred that the reduction of the number of Si−O−Si bonds in the silica backbone with only 15 mol % DMDES increased the ability to deform and to recover from compressive strain. No additional gain in recovery was observed with 45 mol % DMDES, possibly because of greater loss of silanes at high concentration as already discussed. The recovery behavior of aerogels with BTMSPA is identical to results obtained with alkyl-linked silanes. BTMSPA alone results in near perfect elastic recovery while increasing DMDES mole fraction in BTMSPA aerogels contributed to

slightly larger unrecovered strains of 4−6%. Nevertheless, the best combination of high modulus with good recovery was obtained with epoxy-reinforced aerogels with 15% DMDES and APTES. However, it must be noted that this combination produces epoxy-reinforced aerogels with lower surface areas.

3. CONCLUDING REMARKS AND FUTURE DIRECTIONS

In conclusion, the mechanical properties and other characteristics of silica aerogels must be tailored to match the demand of future applications. This includes not only improving strength by reinforcement through the addition of polymer as a conformal coating on the silica nanoskeleton, but also improving their elasticity and flexibility. Most aerogel articles are expected to encounter compressive and bending stresses and be subjected to small strains usually less than 25%. Consequently, the flexibility of the aerogel networks is crucial in such applications. As discussed above, the use of organo-silanes of both types, incorporated into the silica backbone produced promising results.

Of course, tailoring mechanical properties of aerogels depends strongly on proper selection of silane precursors and reaction conditions to achieve complete conversion and incorporation of those precursors. We investigated three alkyl-linked bis-silanes and one silane capable of making only two Si−O−Si bonds per molecule. All of these precursors improve elastic recovery of the aerogels with as little as 15 mol % included in the silica backbone. However, additional incorporation reduces the compressive modulus as was seen in aerogels made with as much as 45 mol % silicon from DMDES or any of the alkyl-linked bis-silanes. Formulations made including APTES as an amine site for epoxy cross-linking and 15 mol % silicon from any of the bis-silanes provided aerogels with both higher compressive modulus and recovery from compression. The data indicated that the hexyl-linked bis-silane (BTMSH) is most effective among the bis-silanes used in this work. Only BTMSH produced aerogels with high mass yields, indicating complete hydrolysis and condensation under the reaction conditions studied. It is possible that fine-tuning reaction conditions for other alkyl linked bis-silanes or DMDES will allow for more complete condensation with these other precursors, leading to similar property enhancement. The use of BTMSPA, an alkyl-linked bis-silane incorporating a secondary amine for cross-linking with epoxy, was seen to allow near complete recovery from compression on its own without incorporating other alkyl-linked silanes or DMDES. Aerogels made using BTMSPA instead of APTES also tended to have higher surface areas

Additional work is still required to make polymer-reinforced silica aerogel articles in a more streamlined process, in commercial scale and in configurations such as flexible thin sheets so that they can be easily wrapped around pipes, tanks or other assemblages needing insulation, or used as flexible insulation for space suits or inflatable structures. Production of optimum formulations discussed herein in thin film form is under investigation. Another area of interest is to study the effectiveness of cage-shaped silanes available in the form of polyhedral oligomeric silsesquioxane (POSS). These molecules have recently been effectively used as cross-linkers in synthesis of flexible and foldable polyimide aerogels.[92] In the context of silica aerogels, POSS molecules carrying between 2 and 4 silanol groups have the potential to bridge the junctions between secondary particles and consequently to reinforce silica networks. A study on this is currently underway and will be reported soon.

AUTHOR INFORMATION

Corresponding Author

*E-mail: maryann.meador@nasa.gov (M.A.B.M.); janas@uakron.edu (S.C.J.).

Present Addresses

‡Currently at AkzoNobel.

ACKNOWLEDGMENT

We thank the Fundamental Aeronautics Program (Subsonics Rotary Wing and Hypersonics) and the NASA Graduate Student Researcher Program for funding this work. We also thank Ms. Linda McCorkle for providing SEM analysis, Mr. Dan Schieman for thermal analysis and helium pycnometry measurements, and Ms. Anna Palczer and Dr. Baochau Nguyen for nitrogen porosimetry results.

REFERENCES

(1) Pierre, A. C.; Pajonk, G. M. *Chem. Rev.* **2002**, *102*, 4243–4265.
(2) Soleimani-Dorcheh, A.; Abbasi, M. H. *J. Mater. Process. Technol.* **2008**, *199*, 10–26.
(3) Daniel, C.; Giudice, S.; Guerra, G. *Chem. Mater.* **2009**, *21*, 1028–1034.
(4) Cardea, S.; Gugliuzza, A.; Sessa, M.; Aceto, M. C.; Drioli, E.; Reverchon, E. *ACS Applied Mater. Interfaces* **2009**, *1*, 171–180.
(5) Liang, C.; Sha, G.; Guo, S. *J. Non-Cryst. Solids* **2000**, *271*, 167–170.
(6) Biesmans, G.; Mertens, A.; Duffours, L.; Woignier, T.; Phalippou, J. *J. Non-Cryst. Solids* **1998**, *225*, 64–68.
(7) Walendziewski, J.; Stolarski, M. *React. Kinet. Catal. Lett.* **2000**, *71*, 201–207.
(8) Tamon, H.; Sone, T.; Mikami, M.; Okazaki, M. J. *Colloid Interface Sci.* **1997**, *188*, 493–500.
(9) Osaki, T.; Hoiuchi, T.; Sugiyama, T.; Suzuki, K.; Mori, T. *J. Non-Cryst. Solids* **1998**, *225*, 111–114.
(10) Leventis, N.; Vassilaras, P.; Fabrizio, E. F.; Dass, A. J. *Mater. Chem.* **2007**, *17*, 1502–1508.
(11) Johnson, J. R., III; Spikowski, J.; Schiraldi, D. A. *ACS Appl. Mater. Interfaces* **2009**, *1*, 1305–1309.
(12) Bandi, S.; Bell, M.; Schiraldi, D. A. *Macromolecules* **2005**, *38*, 9216–9220.
(13) Tamon, H.; Ishizaka, H.; Mikami, M.; Okazaki, M. *Carbon* **1997**, *35*, 791–796.
(14) Kistler, S. S. *Nature* **1931**, *127*, 741–741.
(15) Kistler, S. S. *J. Phys. Chem.* **1932**, *36*, 52–64.
(16) Nicolaon, G. A.; Teichner, S. J. *Bull. Soc. Chim. Fr.* **1968**, 1900.
(17) Tewari, P. H.; Hunt, A. J.; Lofftus, K. D. *Mater. Lett.* **1985**, *3*, 363.
(18) Hrubesh, L. W., *Chem. Ind.* **1990**, Dec *17*, 824-827.
(19) Zhang, G.; Dass, A.; Rawashdeh, A.-M. M.; Thomas, J.; Counsil, J. A.; Sotiriou-Leventis, C.; Fabrizio, E. F.; Ilhan, F.; Vassilaras, P.; Scheiman, D.; McCorkle, L.; Palczer, A.; Johnston, J. C.; Meador, M. A.; Leventis, N. *J. Non-Cryst. Solids* **2004**, *350*, 152–164.
(20) Tsou, P. *J. Non-Cryst. Solids.* **1995**, *186*, 415–427.
(21) Tsou, P.; Brownlee, D. E.; Sandford, S. A.; Hörz, F.; Zolensky, M. E. *J. Geophys. Res.* **2003**, *108*, 8113.
(22) Alexa, L. C.; Huber, G. M.; Lolos, G. J.; Farzanpay, F.; Garibaldi, F.; Jodice, M.; Leone, A.; Perrino, R.; Papandreou, Z.; Humphrey, D. L.; Ulmer, P.; DeLeo, R. *Nucl. Instrum. Methods Phys. Res., Sect. A* **1995**, *365*, 299–307.
(23) Cantin, M.; Casse, M.; Koch, L.; Jouan, R.; Mestran, P.; Roussel, D.; Bonnin, F.; Moutel, J.; Teichner, S. J. *Nucl. Instrum. Methods* **1974**, *118*, 177–182.

(24) daCunha, J. P.; Neves, P.; Lopes, M. *Nucl. Instrum. Methods Phys. Res., Sect. A* **2000**, *452*, 401–421.
(25) Rubin, M.; Lampert, C. M. *Solar Energy Mater.* **1983**, *7*, 393–400.
(26) Wittwer, V. *J. Non-Cryst. Solids* **1992**, *145*, 233–236.
(27) Fricke, J.; Emmerling, A. *J. Sol−Gel Sci.Technol.* **1998**, *13*, 299–303.
(28) Gronauer, M.; Fricke, J. *Acoustica* **1986**, *59*, 177.
(29) Gerlach, R.; Kraus, O.; Fricke, J.; Eccardt, P.-Ch; Kroemer, N.; Magori, V. *J. Non-Cryst. Solids* **1992**, *145*, 227–232.
(30) Gibiat, V.; Lefeuvre, O.; Woignier, T.; Pelous, J.; Phalippou, J. *J. Non-Cryst. Solids* **1995**, *186*, 244–255.
(31) Owens, B. B.; Passerini, S.; Smyrl, W. H. *Electrochim. Acta* **1999**, *45*, 215–224.
(32) Long, J. W.; Swider Lyons, K. E.; Stroud, R. M.; Rolison, D. R. *Electrochem Solid-State Lett.* **2000**, *3*, 453–456.
(33) Pajonk, G. M. *Appl. Catal.* **1991**, *72*, 217–266.
(34) Ward, D. A.; Ko, E. I. *Ind. Eng. Chem. Res.* **1995**, *34*, 421–433.
(35) Ayers, M. R.; Hunt, A. J. *J. Non-Cryst. Solids.* **1998**, *225*, 343–347.
(36) Wang, C.-T.; Wu, C.-L.; Chen, I.-C.; Huang, Y.-H. *Sens. Actuators, B* **2005**, *107*, 402–410.
(37) Jones, S. M. *J. Sol−Gel Sci. Technol.* **2006**, *40*, 351–357.
(38) *Final Report on Advanced Extravehicular Activity Systems Requirements Definition Study*; Report NAS9−17779; Essex Corporation: Colombia, MD, 1989, .
(39) Paul, H. L.; Diller, K. R. *J. Biomech. Eng.* **2003**, *125* 639–647.
(40) Tang, H. H.; Orndoff, E. S.; Trevino, L. A. *36th International Conference on Environment Systems*; Norfolk, VA, July 17−20, 2006; American Institute of Aeronautics and Astronautics: Reston, VA, 2006; 2006-01-2235.
(41) Del Corso, J. A.; Bruce, W. E.; Liles, K. A.; Hughes., S. J. *20th AIAA Aerodynamic Decelerator Systems Technology Conference and Seminar*; Seattle, WA, May 4−7, 2009; American Institute of Aeronautics and Astronautics: Reston, VA, 2009; 2009-2925.
(42) Braun, R. D.; Manning, R. M. *J. Spacecr. Rockets* **2007**, *44*, 310–323.
(43) Brown, G. J.; Lingard, J. S.; Darley, G. D.; Underwood, J. C. *19th AIAA Aerodynamic Decelerator Systems Technology Conference and Seminar*; Williamsburg, VA, May 21−24, 2007; American Institute of Aeronautics and Astronautics: Reston, VA, 2007; 2007-2543.
(44) Reza, S.; Hund, R.; Kustas, F.; Willcockson, W.; Songer, J. *19th AIAA Aerodynamic Decelerator Systems Technology Conference and Seminar*; Williamsburg, VA, May 21−24, 2007; American Institute of Aeronautics and Astronautics: Reston, VA, 2007; 2007-2516.
(45) Fesmire, J. E. *Cryogenics* **2006**, *46*, 111–117.
(46) Fricke, J. *J. Non-Cryst. Solids* **1988**, *100*, 169–173.
(47) Pekala, R. W.; Hrubesh, L. W.; Tillotson, T. M.; Alviso, C. T.; Poco, J. F.; LeMay, J. D. *MRS Symposium W: Scaling in Disordered Materials*; Boston, November 1990; Materials Research Society: Warrendale, PA, 1990.
(48) Gross, J.; Fricke, J. *Nanostruct. Mater.* **1995**, *6*, 905–908.
(49) Woignier, T.; Reynes, J.; HafidiAlaoui, A.; Beurroies, I.; Phalippou, J. *J. Non-Cryst. Solids* **1998**, *241*, 45–52.
(50) Miner, M. R.; Hosticka, B.; Norris, P. M. *J. Non-Cryst. Solids* **2004**, *350*, 285–289.
(51) Iler, R. K. *The Chemistry of Silica*; Wiley: New York, 1979.
(52) Reichenauer, G. *J. Non-Cryst. Solids* **2004**, *350*, 189–195.
(53) Strom, R. A.; Masmoudi, Y.; Rigacci, A.; Petermann, G.; Gullberg, L.; Chevalier, B.; Einarsrud, M.-A. *J. Sol−Gel Sci. Technol.* **2007**, *41*, 291–298.
(54) He, F.; Zhao, H.; Qu, X.; Zhang, C.; Qiu, W. *J. Mater. Process. Technol.* **2009**, *209*, 1621–1626.
(55) Lucas, E. M.; Doescher, M. S.; Ebenstein, D. M.; Wahl, K. J.; Rolison, D. R. *J. Non-Cryst. Solids* **2004**, *350*, 244–252.
(56) Kramer, S. J.; Rubio-Alonso, F.; Mackenzie, J. D. *Mater. Res. Soc. Proc.* **1996**, *435*, 295–299.
(57) Novak, B. M.; Auerbach, D.; Verrier, C. *Chem. Mater.* **1994**, *6*, 282–286.
(58) Wei, T. Y.; Lu, S. Y.; Chang, Y. C. *J. Phys. Chem. B* **2008**, *112*, 11881–11886.
(59) Martin, J.; Hosticka, B.; Lattimer, C.; Norris, P. M. *J. Non-Cryst. Solids* **2001**, *285*, 222–229.
(60) Leventis, N.; Sotiriou-Leventis, C.; Zhang, G.; Rawashdeh, A.-M. M. *Nano Lett.* **2002**, *2*, 957–960.
(61) Leventis, N.; Meador, M. A. B.; Johnston, J. C.; Fabrizzio, E. F.; Ilhan, F. U.S. Patent 7 732 496; June 8, 2010.
(62) Husing, N.; Schubert, U.; Mezer, R.; Fratzl, P.; Riegel, B.; Kiefer, W.; Kohler, D.; Mader, W. *Chem. Mater.* **1999**, *11*, 4.
(63) Meador, M. A. B.; Fabrizzio, E. F.; Ilhan, F.; Dass, A.; Zhang, G.; Vassilaras, P.; Johnston, J. C.; Leventis, N. *Chem. Mater.* **2005**, *17*, 1085–1098.
(64) Katti, A.; Shimpi, N.; Roy, S.; Lu, H.; Fabrizio, E. F.; Dass, A.; Capadona, L. A.; Leventis, N. *Chem. Mater.* **2006**, *18*, 285–296.
(65) Meador, M. A.; Capadona, L. A.; McCorkle, L.; Papadopoulos, D. S.; Leventis, N. *Chem. Mater.* **2007**, *19*, 2247–2260.
(66) Lee, O. J.; Lee, K.-H.; Yim, T. J.; Kim, S. Y.; Yoo, K.-P. *J. Non-Cryst. Solids* **2002**, *298*, 287–292.
(67) Jensen, K. I.; Schultz, J. M.; Kristiansen, F. H. *J. Non-Cryst. Solids* **2004**, *350*, 351–357.
(68) Deng, Z.; Wang, J.; Wei, J.; Bao, Y.; Shen, J.; Chen, L. *High Temp.−High Pressures* **2001**, *33*, 135–140.
(69) Ilhan, U. F.; Fabrizio, E. F.; McCorkle, L.; Scheiman, D. A.; Dass, A.; Palczer, A.; Meador, M. A. B.; Johnston, J. C.; Leventis, N. *J. Mater. Chem.* **2006**, *16*, 3046–3054.
(70) Mulik, S.; Sotiriou-Leventis, C.; Churu, G.; Lu, H.; Leventis, N. *Chem. Mater.* **2008**, *20* (15), 5035–5046.
(71) Nguyen, B. N.; Meador, M. A. B.; Tousley, M. E.; Shonkwiler, B.; McCorkle, L.; Scheiman, D. A.; Palczer, A. *ACS Appl. Mater. Interfaces* **2009**, *1*, 621–630.
(72) Boday, D. J.; Stover, R. J.; Muriithi, B.; Keller, M. W.; Wertz, J. T.; Obrey, K. A. D.; Loy, D. A. *ACS Appl. Mater. Interfaces* **2009**, *1*, 1364–1369.
(73) Boday, D. J.; Stover, R. J.; Muriithi, B.; Keller, M. W.; Wertz, J. T.; Obrey, K. A. D.; Loy, D. A. *Chem. Mater.* **2008**, *20*, 2845–2847.
(74) Meador, M. A. B.; Vivod, S. L.; McCorkle, L.; Quade, D.; Sullivan, R. M.; Ghosn, L. J.; Clark, N.; Capadona, L. A. *J. Mater. Chem.* **2008**, *18*, 1843–1852.
(75) Meador, M. A. B.; Weber, A. S.; Hindi, A.; Naumenko, M.; McCorkle, L.; Quade, D.; Vivod, S. L.; Gould, G. L.; White, S.; Deshpande, K. *ACS Appl. Mater. Interfaces* **2009**, *1*, 894–906.
(76) Meador, M. A. B.; Scherzer, C. M.; Nguyen, B. N.; Quade, D.; Vivod, S. L. *ACS Appl. Mater. Interfaces* **2010**, *2*, 2162–2168.
(77) Capadona, L. A.; Meador, M. A. B.; Alunni, A.; Fabrizio, E. F.; Vassilaras, P.; Leventis, N. *Polymer* **2006**, *47*, 5754–5761.
(78) Li, L.; Yalcin, B.; Nguyen, B. N.; Meador, M. A. B.; Cakmak, M. *ACS Appl. Mater. Interfaces* **2009**, *1* (11), 2491–2501.
(79) Rao, A. V.; Bhagat, S. D.; Hirashima, H.; Pajonk, G. M. *J. Colloid Interface Sci.* **2006**, *300*, 279.
(80) Kanamori, K.; Aizawa, M.; Nakanishi, K.; Hanada, T. *Adv. Mater.* **2007**, *19*, 1589–1593.
(81) Bhagat, S. D.; Oh, C.-S.; Kim, Y.-H.; Ahn, Y.-S.; Yeo, J.-G. *Microporous Mesoporous Mater.* **2007**, *100*, 350–355.
(82) Nguyen, B. N.; Meador, M. A. B.; Medoro, A.; Arendt, V.; Randall, J. P.; McCorkle, L.; Shonkwiler, B. *ACS Appl. Mater. Interfaces* **2009**, *2*, 1430–1443.
(83) Guo, H.; Nguyen, B. N.; McCorkle, L. S.; Shonkwiler, B.; Meador, M. A. B. *J. Mater. Chem.* **2009**, *19*, 9054–9062.
(84) Shea, K. J.; Loy, D. A. *Chem. Mater.* **2001**, *13*, 3306–3319.
(85) Shea, K. J.; Loy, D. A. *Acc. Chem. Res.* **2001**, *34*, 707–716.
(86) Loy, D. A.; Shea, K. J. *Chem. Rev.* **1995**, *95*, 1431–1442.
(87) Schaefer, D. W.; Beaucage, G.; Loy, D. A.; Shea, K. J.; Lin, J. S. *Chem. Mater.* **2004**, *16*, 1402–1410.

(88) Loy, D. A.; Jamison, G. M.; Baugher, B. M.; Russick, E. M.; Assink, R. A.; Prabakar, S.; Shea, K. J. *J. Non-Cryst. Solids* **1995**, *186*, 44–53.

(89) Note that this process can be shortened a great deal, but the study was done using this protocol to be consistent with previous studies.

(90) Oviatt, H. W.; Shea, K. J.; Small, J. H. *Chem. Mater.* **1993**, *5*, 943–950.

(91) It should be noted that prior work[75] showed that epoxy-reinforced aerogels with similar amounts of APTES and no bis-silanes could be deformed to 25% strain without brittle failure. Slightly different reaction conditions, such as lower water to silane ratio and higher acid concentrations used in the current study is probably responsible for the difference in deformation behavior. In any case, BTMSH was still seen to decrease unrecovered strain in the epoxy-reinforced aerogels to a similar extent.

(92) Guo, H.; Meador, M. A. B.; McCorkle, L.; Quade, D. J.; Guo, J.; Hamilton, B.; Cakmak, M.; Sprowl, G. *ACS Appl. Mater. Interfaces* **2011**, *3*, dx.doi.org/10.1021/am101123h.